

SN 2017CFD: A NORMAL TYPE IA SUPERNOVA DISCOVERED VERY YOUNG

XUHUI HAN¹, WEIKANG ZHENG², BENJAMIN E. STAHL^{2,3,4}, JAMISON BURKE^{5,6}, JOZSEF VINKO^{7,8,9}, THOMAS DE JAEGER^{2,10}, THOMAS G. BRINK², BORBALA CSEH⁷, DAICHI HIRAMATSU^{5,6}, D. ANDREW HOWELL^{5,6}, BERNADETT IGNACZ⁷, REKA KONYVES-TOH⁷, MATE KREZINGER⁷, CURTIS MCCULLY^{5,6}, ANDRAS ORDASI⁷, DORA PINTER⁷, KRISZTIAN SARNECZKY⁷, ROBERT SZAKATS⁷, KEVIN TANG², KRISZTIAN VIDA⁷, JING WANG^{1,11}, JIANYAN WEI¹, J. CRAIG WHEELER^{9,12}, LIPING XIN¹, AND ALEXEI V. FILIPPENKO^{2,13}*Draft version March 3, 2022*

ABSTRACT

The Type Ia supernova (SN Ia) 2017cfd in IC 0511 (redshift $z = 0.01209 \pm 0.00016$) was discovered by the Lick Observatory Supernova Search 1.6 ± 0.7 d after the fitted first-light time (FFLT; 15.2 d before B -band maximum brightness). Photometric and spectroscopic follow-up observations show that SN 2017cfd is a typical, normal SN Ia with a peak luminosity $M_B \approx -19.2 \pm 0.2$ mag, $\Delta m_{15}(B) = 1.16$ mag, and reached a B -band maximum ~ 16.8 d after the FFTL. We estimate there to be moderately strong host-galaxy extinction ($A_V = 0.39 \pm 0.03$ mag) based on MLCS2k2 fitting. The spectrum reveals a Si II $\lambda 6355$ velocity of $\sim 11,200$ km s⁻¹ at peak brightness. SN 2017cfd was discovered very young, with multiband data taken starting 2 d after the FFTL, making it a valuable complement to the currently small sample (fewer than a dozen) of SNe Ia with color data at such early times. We find that its intrinsic early-time $(B - V)_0$ color evolution belongs to the "blue" population rather than to the distinct "red" population. Using the photometry, we constrain the companion star radius to be $\lesssim 2.5 R_\odot$, thus ruling out a red-giant companion.

Subject headings: supernovae: general — supernovae: individual (SN 2017cfd)

1. INTRODUCTION

Type Ia supernovae (SNe Ia; see Filippenko 1997 for a review of supernova classification) are the thermonuclear runaway explosions of carbon/oxygen white dwarfs (see, e.g., Hillebrandt & Niemeyer 2000 for a review). One of the most important applications of SN Ia is that they can be used as standardizable candles for measurements of the expansion rate of the Universe (Riess et al. 1998; Perlmutter et al. 1999). The have also provided the main initial evidence for "H₀ tension" — the discrepancy in the values of H₀ measured locally and inferred from Planck (e.g., Riess et al. 2018, 2019).

There are two general favored progenitor systems for SNe Ia: the single-degenerate scenario (Hoyle & Fowler 1960; Hachisu et al. 1996; Meng et al. 2009; Röpke et al. 2012), which consists of a single white dwarf accreting material from a companion, and the double-degenerate scenario involving the merger of two white dwarfs (Webbink 1984; Iben & Tutukov 1984; Pakmor et al. 2012; Röpke et al. 2012). However, our understanding of the progenitor systems and explosion mechanisms remains substantially incomplete both theoretically and observationally (see a recent review by Jha et al. 2019).

Extremely early discovery and follow-up observations are essential for understanding the physical properties of SNe Ia and for revealing their progenitor systems. For example, early-time light curves can be used to constrain the companion-star radius, as in the cases of SN 2011fe (Nugent et al. 2011; Bloom et al. 2012), SN 2012cg (Silverman et al. 2012b), SN 2013dy (Zheng et al. 2013), SN 2013gy (Holmbo et al. 2019), SN 2014J (Goobar et al. 2014), iPTF14atg (Cao et al. 2015), SN 2015F (Im et al. 2015), SN 2017cbv (Hosseinizadeh et al. 2017), SN 2018oh (Li et al. 2019), and SN 2019ein (Kawabata et al. 2019), although there are other alternatives to explain the data (e.g., Piro & Nakar 2013; Maeda et al. 2018; Magee et al. 2018; Stritzinger et al. 2018a; Polin et al. 2019). They can also be used to explore the "dark phase" of SN Ia, which can last for a few hours to days between the moment of explosion and the first observed light (Rabinak, Livne, & Waxman 2012; Piro & Nakar 2013, 2014), as with SN 2014J (Goobar et al. 2014), SN 2015F (Im et al. 2015), and iPTF14pdk (Cao et al. 2016). Optical spectra obtained shortly after explosion can be used to examine the possible unburned material from the progenitor white dwarf, such as the C II feature, which was found significantly only in the very early spec-

¹ Key Laboratory of Space Astronomy and Technology, National Astronomical Observatories, Chinese Academy of Sciences, Beijing 100101, China (email: hxxh@nao.cas.cn).

² Department of Astronomy, University of California, Berkeley, CA 94720-3411, USA (email: weikang@berkeley.edu).

³ Department of Physics, University of California, Berkeley, CA 94720, USA.

⁴ Marc J. Staley Graduate Fellow.

⁵ Las Cumbres Observatory Global Telescope Network, 6740 Cortona Dr Ste 102, Goleta, CA 93117-5575, USA.

⁶ Department of Physics, University of California, Santa Barbara, CA 93106-9530, USA.

⁷ Konkoly Observatory, Institute for Astronomy and Earth Sciences, Konkoly Thege ut 15-17, Budapest, 1121 Hungary.

⁸ Department of Optics and Quantum Electronics, University of Szeged, Dom ter 9, Szeged, 6720, Hungary.

⁹ Department of Astronomy, University of Texas, 2515 Speedway, Austin, TX 78712, USA.

¹⁰ Bengier Postdoctoral Fellow.

¹¹ Guangxi Key Laboratory for Relativistic Astrophysics, School of Physical Science and Technology, Guangxi University, Nanning 530004, China.

¹² George P. and Cynthia Woods Mitchell Institute for Fundamental Physics & Astronomy, Texas A&M University, Department of Physics and Astronomy, 4242 TAMU, College Station, TX 77843, USA.

¹³ Miller Senior Fellow, Miller Institute for Basic Research in Science, University of California, Berkeley, CA 94720, USA.

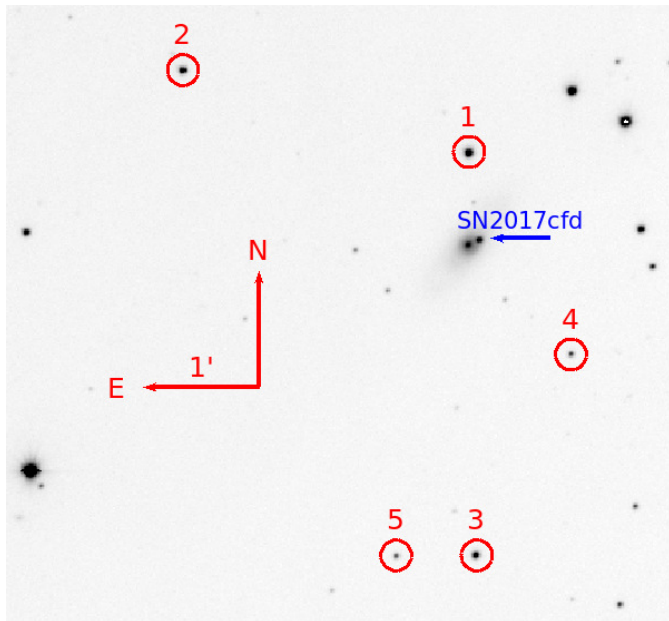


FIG. 1.— KAIT unfiltered image showing the location of SN 2017cfd. Five reference stars are also marked with circles. tra of SN 2013dy (Zheng et al. 2013) and SN 2017cbv (Hossein-zadeh et al. 2017).

Observationally, numerous efforts have been conducted to discover young SNe Ia, with progressively more surveys joining in the past few years (e.g., All-Sky Automated Survey for Supernovae, Asteroid Terrestrial-impact Last Alert System, Palomar Transient Factory, Intermediate Palomar Transient Factory). In 2011, to discover very young SNe Ia (hours to days after explosion), our Lick Observatory Supernova Search (LOSS; Filippenko et al. 2001; Filippenko 2005; Leaman et al. 2011) modified its search strategy. Since that year, using the 0.76 m Katzman Automatic Imaging Telescope (KAIT), our group monitored fewer galaxies but with a higher cadence. Consequently, our group has discovered many young SNe Ia in the past few years (see Section 3.4). Among these discoveries is SN 2017cfd, which was discovered merely 1.6 ± 0.5 d after the fitted first-light time (FFLT), and KAIT automatically started multi-band follow-up observations only minutes after discovery. Here we present our optical photometry and spectroscopy together with an analysis.

2. DISCOVERY AND OBSERVATIONS

SN 2017cfd was discovered in an 18 s unfiltered KAIT image taken at 06:32:37 on 2017 March 16 (UT dates are used throughout this paper), at ~ 19 mag in the *Clear* band (close to the *R* band; see Li et al. 2003). It was reported to the Transient Name Server (TNS) shortly after discovery by Halle, Zheng, & Filippenko¹⁴. We measure its J2000 coordinates to be $\alpha = 08^{\text{h}}40^{\text{m}}49.09^{\text{s}}$, $\delta = +73^{\circ}29'15''.1$, with an uncertainty of $\pm 0''.5$ in each coordinate. SN 2017cfd is $5''.8$ west and $3''.1$ north of the nucleus of the host galaxy IC 0511, which has redshift $z = 0.01209 \pm 0.00016$ (Falco et al. 1999) and a spiral morphology (S0/a; de Vaucouleurs et al. 1991).

KAIT automatically performed multiband photometric follow-up observations of SN 2017cfd once it was

discovered. KAIT data were reduced using our image-reduction pipeline (Ganeshalingam et al. 2010; Stahl et al. 2019a). We applied an image-subtraction procedure to remove the host-galaxy light, and point-spread-function (PSF) photometry was then obtained using DAOPHOT (Stetson 1987) from the IDL Astronomy User’s Library¹⁵. The multiband data are calibrated to local Pan-STARRS1¹⁶ stars (see Figure 1), whose magnitudes were first transformed into the Landolt system using the empirical prescription presented by Tonry et al. (2012, Equation 6) and then transformed to the KAIT natural system. Apparent magnitudes were all measured in the KAIT4 natural system. The final results were transformed to the standard system using local calibrators and color terms for KAIT4 (Stahl et al. 2019a).

Note that KAIT photometry of SN 2017cfd has already been published by Stahl et al. (2019a). The major difference between our reanalysis presented here compared to the results of Stahl et al. (2019a) is that we performed a more careful analysis of the data obtained on the discovery night, where multiple short exposures were taken for each filter. Considering that the SN was very faint ($B \approx 19.2$ mag) on the discovery night, here we coadd the short-exposure images in each filter in order to increase the signal-to-noise ratio before applying subtraction and further analysis, whereas the Stahl et al. pipeline¹⁷ did the photometry on each single image and then took the average. We also added two epochs of upper-limit measurements in the *Clear* band prior to discovery.

Additional photometric data were obtained with the 0.6/0.9 m Schmidt telescope, equipped with a front-illuminated FLI Proline PL16801 4096×4096 pixel CCD and Johnson-Cousins *BVRI* filters, at Piskésető Mountain Station of Konkoly Observatory, between 2017-03-17 and 2017-05-28. The CCD frames were reduced using standard *IRAF*¹⁸ tasks. Template frames were taken with the same instrument and setup on 2019-03-23 and 2019-03-24, 2 yr after peak brightness, when the SN had faded sufficiently below the detection limit. Subtraction of the templates was computed using self-developed *IRAF* scripts. After that, PSF photometry of the SN was performed on the subtracted frames, while the determination of the PSF on each frame and photometry of local comparison stars were done on the original (dark- and flatfield-corrected) frames. Finally, the instrumental magnitudes were transformed to the standard Johnson-Cousins system using PS1-photometric data¹⁹ for the local comparison stars.

Photometric reduction for the Las Cumbres Observatory (LCO; Brown et al. 2013) images was accomplished using *lcogtspipe* (Valenti et al. 2016), a PyRAF-based pipeline. Image subtraction was accomplished using *PyZOGY* (Guevel & Hossein-zadeh 2017), an implementation in Python of the subtraction algorithm described by Zackay et al. (2016).

¹⁵ <http://idlastro.gsfc.nasa.gov/>

¹⁶ <http://archive.stsci.edu/panstarrs/search.php>

¹⁷ <https://github.com/benstahl92/LOSSPhotPypeline>

¹⁸ *IRAF* is distributed by the National Optical Astronomy Observatories, which are operated by the Association of Universities for Research in Astronomy, Inc., under cooperative agreement with the US National Science Foundation.

¹⁹ <http://archive.stsci.edu/panstarrs/search.php>

¹⁴ <https://wis-tns.weizmann.ac.il/object/2017cfd>

TABLE 1
MULTIBAND PHOTOMETRY OF SN 2017CFD

MJD	Mag	1 σ	Mag	1 σ	Mag	1 σ	Mag	1 σ	Mag	1 σ
From KAIT	<i>B</i>		<i>V</i>		<i>R</i>		<i>I</i>		<i>Clear</i>	
57825.322	-	-	-	-	-	-	-	-	>19.0	-
57826.310	-	-	-	-	-	-	-	-	>19.1	-
57828.278	19.24	0.36	19.09	0.17	-	-	-	-	19.10	0.26
57829.172	17.71	0.14	18.69	0.76	16.87	0.15	18.37	0.27	17.82	0.13
57830.322	17.06	0.05	17.09	0.06	16.80	0.07	16.38	0.10	17.16	0.10
57831.279	17.18	0.24	16.91	0.22	16.29	0.18	16.68	0.39	16.57	0.09
57841.275	14.81	0.19	14.97	0.02	-	-	-	-	14.68	0.02
57843.241	-	-	-	-	-	-	-	-	14.67	0.02
57845.232	14.96	0.01	14.84	0.01	14.73	0.03	15.05	0.02	14.82	0.03
57864.221	-	-	-	-	-	-	-	-	15.88	0.06
57872.189	-	-	-	-	-	-	-	-	16.31	0.10
57840.311	15.06	0.01	14.98	0.01	14.77	0.02	14.85	0.02	15.07	0.06
57844.297	14.98	0.01	14.86	0.01	14.72	0.01	14.99	0.03	14.68	0.02
57849.259	-	-	-	-	-	-	-	-	15.25	0.14
57853.276	15.57	0.22	15.16	0.02	15.19	0.03	15.32	0.06	15.44	0.06
57878.204	-	-	-	-	-	-	-	-	16.73	0.16
57881.215	18.82	0.22	16.85	0.08	15.92	0.06	15.56	0.06	17.04	0.18
57883.207	18.52	0.17	17.04	0.07	16.28	0.24	15.58	0.07	16.96	0.13
57887.185	19.02	0.28	17.36	0.23	-	-	-	-	-	-
57889.197	19.35	0.24	17.29	0.12	16.65	0.11	15.83	0.14	-	-
57891.200	18.80	0.14	17.68	0.11	16.62	0.06	-	-	17.30	0.12
57893.194	-	-	-	-	-	-	-	-	17.30	0.18
From Konkoly	<i>B</i>		<i>V</i>		<i>R</i>		<i>I</i>			
57829.020	17.96	0.07	17.92	0.06	17.79	0.05	17.41	0.07		
57832.880	16.16	0.02	16.17	0.02	15.90	0.02	15.87	0.03		
57833.900	15.87	0.03	15.85	0.02	15.60	0.02	15.58	0.03		
57835.860	15.42	0.02	15.43	0.02	15.23	0.03	15.15	0.03		
57837.820	15.19	0.04	15.19	0.03	14.95	0.03	14.93	0.03		
57841.860	14.91	0.03	14.86	0.02	14.71	0.02	14.90	0.02		
57849.850	15.20	0.05	14.94	0.04	14.79	0.08	14.97	0.24		
57852.830	15.46	0.03	15.13	0.02	15.10	0.04	15.61	0.06		
57853.830	15.51	0.03	15.22	0.02	15.17	0.03	15.65	0.05		
57857.820	15.95	0.03	15.42	0.01	15.41	0.03	15.62	0.03		
57859.830	16.16	0.04	15.54	0.02	15.55	0.04	15.58	0.03		
57860.830	16.29	0.04	15.60	0.02	15.51	0.03	15.56	0.03		
57867.830	17.11	0.03	15.96	0.02	15.70	0.05	15.49	0.04		
57873.810	17.61	0.04	16.33	0.02	15.87	0.02	15.52	0.03		
57875.840	17.79	0.03	16.48	0.02	16.01	0.02	15.67	0.03		
57877.820	17.92	0.03	16.64	0.03	16.16	0.03	15.86	0.04		
57883.840	18.02	0.08	16.93	0.04	16.48	0.04	16.16	0.03		
57889.860	18.25	0.04	17.09	0.02	16.71	0.03	16.41	0.03		
57899.940	18.52	0.06	17.25	0.04	16.97	0.03	17.10	0.07		
57901.830	18.32	0.03	17.49	0.02	17.19	0.03	17.03	0.04		
From LCO	<i>B</i>		<i>V</i>		<i>g</i>		<i>r</i>		<i>i</i>	
57833.301	16.10	0.01	16.07	0.01	16.00	0.01	16.03	0.02	16.21	0.01
57839.238	15.11	0.02	-	-	-	-	-	-	-	-
57840.193	15.05	0.02	14.98	0.01	14.91	0.01	15.02	0.02	15.36	0.02
57844.262	14.98	0.02	14.82	0.02	14.78	0.01	14.85	0.01	15.51	0.02
57849.256	15.17	0.01	14.91	0.01	14.96	0.02	15.00	0.02	15.72	0.03
57850.155	15.28	0.01	14.98	0.01	15.04	0.01	15.07	0.02	15.79	0.02
57860.225	16.33	0.03	15.57	0.03	15.80	0.01	15.68	0.01	16.35	0.01
57866.179	17.02	0.02	15.92	0.02	16.66	0.02	15.83	0.01	16.20	0.02
57871.193	17.42	0.02	16.25	0.02	17.06	0.02	15.96	0.02	16.11	0.04
57875.186	17.73	0.01	16.55	0.01	17.41	0.01	16.30	0.02	16.34	0.02
57887.124	18.15	0.05	17.19	0.01	17.89	0.02	17.06	0.02	17.26	0.01
57893.117	18.30	0.09	17.43	0.03	18.01	0.02	17.32	0.01	17.67	0.02

In addition, SN 2017cfd was observed by the Foundation Supernova Survey in the g , r , i , and z filters for 6 epochs and published by Foley et al. (2018); we include these data in our light-curve analysis.

We performed spectroscopic follow-up observations of SN 2017cfd, with a total of 12 spectra obtained ranging from 3.5 d to 80 d after the FFLT (-13.2 d to $+62.8$ d relative to B -band maximum brightness). The spectra were taken mainly with the Kast double spectrograph (Miller & Stone 1993) on the Shane 3 m telescope at Lick Observatory and the FLOYDS robotic spectrograph on the LCO 2.0 m Faulkes Telescope North on Haleakala, Hawaii. A single additional spectrum, which is also the earliest one, was taken with the Low Resolution Spectrograph-2 (LRS2; Chonis et al. 2014, 2016) on the 10 m Hobby-Eberly Telescope at McDonald Observatory.

Data were reduced following standard techniques for CCD processing and spectrum extraction using *IRAF*. The spectra were flux calibrated through observations of appropriate spectrophotometric standard stars. All Kast spectra were taken at or near the parallactic angle (Filippenko 1982) to minimize differential light losses caused by atmospheric dispersion, and were reduced using KastShiv²⁰ pipeline. Low-order polynomial fits to calibration-lamp spectra were used to determine the wavelength scale, and small adjustments derived from night-sky emission lines in the target frames were applied. Flux calibration and telluric-band removal were done with our own IDL routines; details are described by Silverman et al. (2012a) and Shivvers et al. (2019).

3. LIGHT-CURVE ANALYSIS

The left panel of Figure 2 shows the multiband light curves of SN 2017cfd from KAIT, LCO, Konkoly, and the Foundation Supernova Survey observations; colors and symbols are coded for different sources, with photometric data listed in Table 1. Data in the BVR and C lear filters are given in the Vega system, while those in the gri filters are given in the AB system. As one can see, we have full photometric coverage from discovery to ~ 80 days thereafter in six optical bands. The light curves show that SN 2017cfd was discovered at a very early time, with its discovery magnitude in the B band > 4 mag below peak brightness. Applying a low-order polynomial fit, we find that SN 2017cfd reached an apparent peak of 14.95 ± 0.03 mag at MJD = 57843.42 in B , and $\Delta m_{15}(B) = 1.16 \pm 0.11$ mag.

3.1. Estimating the First-Light Time

To determine the first-light time t_0 (note that here we find the first-light time rather than the explosion time since the SN may exhibit a "dark phase"), we use a broken-power-law function, presented as Equation 7 of Zheng & Filippenko (2017a), to fit the light curve from the discovery date to ~ 45 days later. Such a function was shown to be mathematically analytic and physically related to the SN parameters (Zheng & Filippenko 2017a). The function has also been applied to fit B light curves of 56 SNe Ia (Zheng et al. 2017b) and R light curves of 256 SNe Ia of R -band (Papadogiannakis et al. 2019). The light curves of SN 2017cfd were fit with all

parameters free, but only the B and V bands, which have the best coverage and also to avoid the second peak in the redder bands. The right panel of Figure 2 shows the best-fit result; we find the FFLT $t_{0(B)} = 57826.64 \pm 0.7$ and $t_{0(V)} = 57826.98 \pm 0.7$, consistent with each other. Since Zheng et al. (2017b) showed with a large sample that the FFLT has smaller scatter in B than in V or other bands, here we adopt the B -band result ($t_0 = 57826.64 \pm 0.7$) for later analysis.

With the FFLT and peak-time values derived above, we estimate the SN 2017cfd rise time to be 16.8 days, very typical for SNe Ia (Zheng et al. 2017b). It also means that the SN was discovered merely 1.6 d after the FFLT, 15.2 d before B -band maximum light. This makes SN 2017cfd one of the earliest detected SNe Ia in addition to other others, such as SN 2009ig (Foley et al. 2012), SN 2011fe (Nugent et al. 2011), SN 2012cg (Silverman et al. 2012b), SN 2013dy (Zheng et al. 2013), SN 2013gy (Holmbo et al. 2019), SN 2014J (Zheng et al. 2014; Goobar et al. 2014), iPTF14atg (Cao et al. 2015), SN 2015F (Im et al. 2015), SN 2017cbv (Hosseinizadeh et al. 2017), SN 2018oh (Li et al. 2019), and SN 2019ein (Kawabata et al. 2019).

3.2. Distance and Extinction

Adopting a standard cosmological model with $H_0 = 73$ km s⁻¹ Mpc⁻¹, $\Omega_M = 0.27$, and $\Omega_\Lambda = 0.73$, as well as $z = 0.01209$, a distance modulus of 33.52 ± 0.15 mag (here labeled as μ_1) is obtained. With $E(B - V)_{MW} = 0.02$ mag (Schlafly & Finkbeiner 2011), this implies that SN 2017cfd has an absolute magnitude of $M_B = -18.6 \pm 0.2$ mag at peak brightness before correcting for host-galaxy extinction. This is somewhat fainter than the typical, normal SN Ia (we expect $M_B \approx -19.4$ mag from the Phillips (1993) relation with the above value of $\Delta m_{15}(B)$); Thus, SN 2017cfd likely suffered a certain amount of host-galaxy extinction. In fact, from the spectra (see Section 4), we clearly see the Na I D absorption feature, which is often converted into reddening (but with large scatter) based on empirical relationships (Poznanski et al. 2011; Stritzinger et al. 2018b). In Section 4, using the equivalent width (EW) of Na I D, we estimate an extinction of $A_V = 1.34 \pm 0.40$ mag and $E(B - V) = 0.45 \pm 0.13$ assuming $R_V = 3.1$. This amount of host extinction appears too high for SN 2017cfd, as discussed above; SN 2017cfd would have a peak absolute magnitude too bright for a normal SN Ia according to the Phillips (1993) relation.

In order to obtain an independent estimate of the host extinction, we performed a MLCS2k2 (Jha et al. 2007) fit to the B , V , R , and I light curves (not including g , r , i , and z as there are no template light curves in the default MLCS2k2 settings) of SN 2017cfd by fixing $R_V = 1.7$ (there are indications that $R_V = 3.1$ overestimates the host-galaxy extinction; e.g., Hicken et al. 2009). The fitting parameters are given in Table 2; we found $\Delta = 0.03 \pm 0.03$, a peak-brightness time of 57843.41 ± 0.08 (consistent with the value derived from the low-order polynomial fit), and $A_V = 0.39 \pm 0.03$ mag. With this amount of host extinction correction, SN 2017cfd has a peak absolute magnitude of $M_B = -19.2 \pm 0.2$ mag, which is now consistent with the expectation from the Phillips relation.

We also performed a SALT2 (Guy et al. 2007) fit-

²⁰ <https://github.com/ishivvers/TheKastShiv>

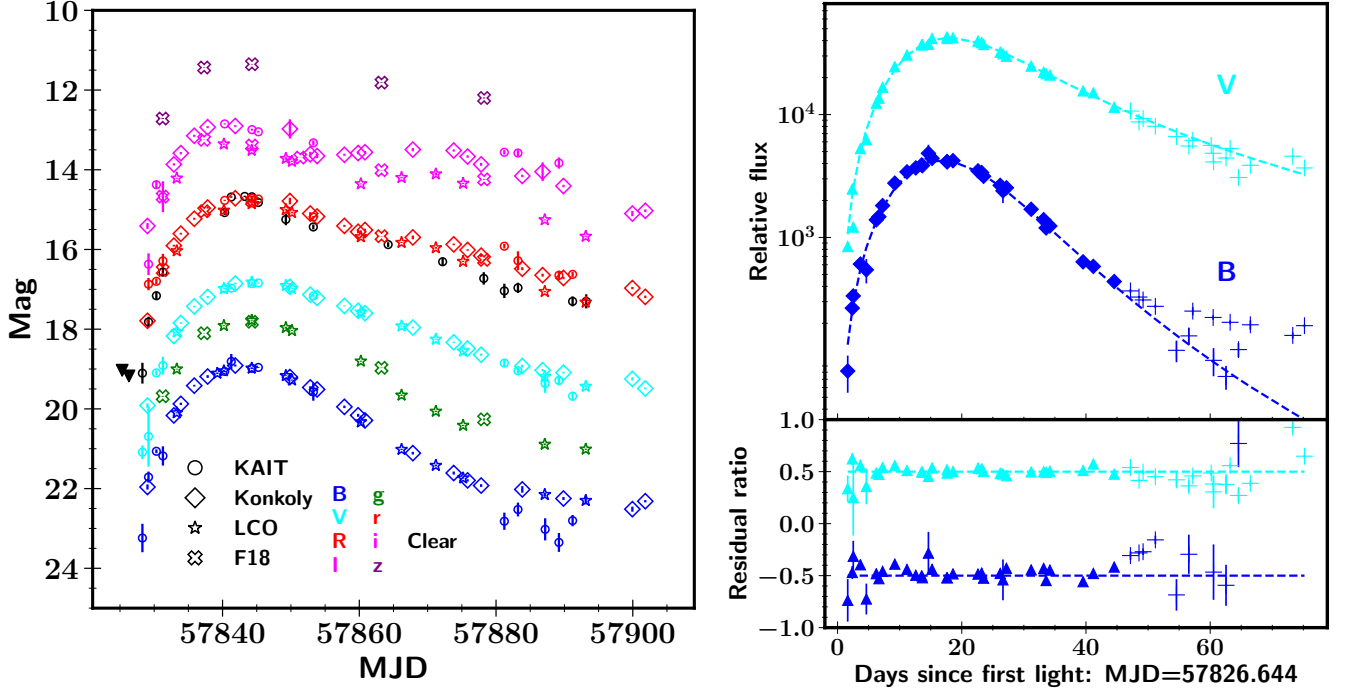


FIG. 2.— Left: Light curve of SN 2017cfd from KAIT, LCO, Konkoly, and the Foundation Supernova Survey observations (labeled as F18); colors and symbols are coded for different filters and sources. The two black solid triangles mark the nondetections from KAIT *Clear* observations one and two days before discovery. Right: *B* and *V* light-curve fitting using the analytic function presented by Zheng & Filippenko (2017a, Equation 7) from discovery to ~ 45 days later. Solid data points are included in the fit while cross-shaped ones are excluded.

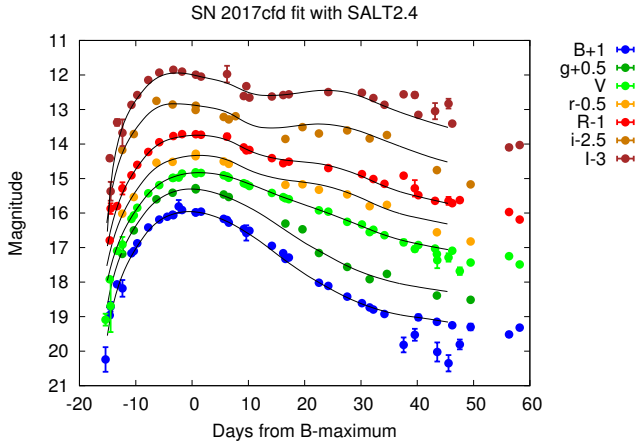


FIG. 3.— SALT2 fitting results to the *BVRIgri* light curves of SN 2017cfd.

ting to the SN 2017cfd light curves. To directly compare with the MLCS2k2 fitting, we first applied the SALT2 fitting with the *B*, *V*, *R*, and *I* light curves. We then applied a second SALT2 fitting to all the *BVRIgri* light curves (as shown in Figure 3); the SALT2 fitting parameters are given in Table 2. As one can see in Figure 3, the SALT2 model provides very good fits to the light curves of SN 2017cfd, and the fitting results are consistent with those of MLCS2k2. The peak time derived from MLCS2k2 fitting and two SALT2 fittings are within 0.3 days, and the distance moduli (all shifted to $H_0 = 73 \text{ km s}^{-1} \text{ Mpc}^{-1}$) derived from MLCS2k2 fitting (μ_2) and two SALT2 fittings (μ_3 and μ_4) are within the 1σ uncertainties; they are also consistent with μ_1 .

Comparing the Na I D EW and MLCS2k2 fitting meth-

ods for estimating the host extinction, MLCS2k2 appears to have a more reasonable result; considering that the Na I D EW method has large scatter, we adopt a host extinction of $A_V = 0.39 \pm 0.03 \text{ mag}$ with $R_V = 1.7$ as our final result for further analysis. Thus, SN 2017cfd has a peak absolute magnitude of $M_B = -19.2 \pm 0.2 \text{ mag}$ (adopting the μ_1 value), after correcting for both the Milky Way extinction and the host extinction.

With a peak magnitude $M_B = -19.2 \pm 0.2 \text{ mag}$, a rise time of 16.8 d, and a Si II $\lambda 6355$ velocity of $\sim 11,200 \text{ km s}^{-1}$ (see Section 4) at peak brightness, we derive M_{v2t2} (as used by Zheng et al. 2018) to be -11.37 , thus putting SN 2017cfd slightly under, but roughly consistent with (given the 2σ uncertainties), the M_p vs. M_{v2t2} relationship presented by Zheng et al. (2018; see the right panel of their Figure 6).

3.3. Pseudobolometric Light Curve

The pseudobolometric light curve of SN 2017cfd was assembled using our *BVRI* photometric data after correcting for redshift, interstellar extinction, and distance. We apply the same procedure as Li et al. (2019) used for SN 2018oh, except that the missing ultraviolet fluxes are estimated by assuming zero flux at 2000 \AA and a linear flux increase between this wavelength and the mid-wavelength of the *B* band. The unobserved infrared fluxes are approximated by attaching a Rayleigh-Jeans tail to the observed *I*-band flux and integrating it between the wavelength of the *I* band and infinity. These approximations are found to be reasonably good representations for the unobserved ultraviolet and infrared parts of the spectral energy distribution (SED) of SNe Ia (Konyves-Toth et al., in prep.).

The pseudobolometric light curve is fit by a modified

TABLE 2
MLCS2k2 AND SALT2 FITTING RESULTS

parameter	value	parameter	value	parameter	value
MLCS2k2 (B, V, R, I)		SALT2 (B, V, R, I)		SALT2 (B, V, R, I, g, r, i)	
μ_2 (mag)	33.59 ± 0.05	μ_3 (mag)	33.58 ± 0.09	μ_4 (mag)	33.70 ± 0.07
Peak time	57843.41 ± 0.08	Peak time	57843.76 ± 0.03	Peak time	54843.64 ± 0.03
Δ	0.03 ± 0.03	C	0.0804 ± 0.0253	C	0.0375 ± 0.0177
A_V (mag)	0.39 ± 0.03	x0	0.0200 ± 0.0005	x0	0.0203 ± 0.0004
		x1	-0.6149 ± 0.0307	x1	-0.6005 ± 0.0240

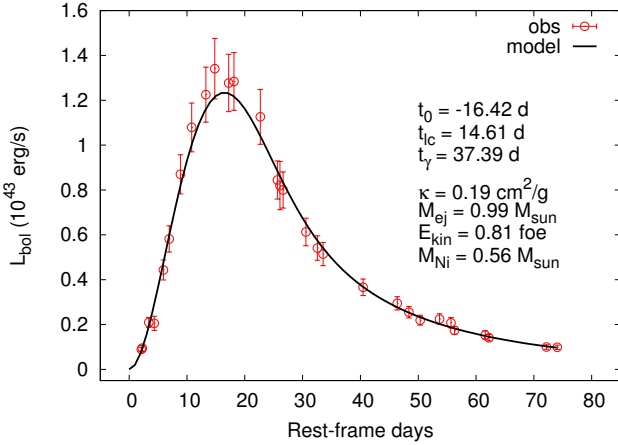


FIG. 4.— Pseudobolometric light-curve fitting of SN 2017cfd assembled using $BVRI$ photometric data after correcting for redshift, interstellar extinction, and distance; see text for details.

Arnett model including partial gamma-ray leaking from the diluting ejecta, assuming $\kappa_\gamma = 0.03 \text{ cm}^2 \text{ g}^{-1}$ (see Li et al. 2019 for details). The best-fit model, found by χ^2 -minimization, has the following parameters: rest-frame days between FFLT and B -band maximum $t_r = 16.42 \pm 0.06$ days, light-curve timescale $t_d = 14.61 \pm 0.27$ days, γ -ray leakage timescale $t_\gamma = 37.39 \pm 0.66$ days, initial mass of radioactive ^{56}Ni $M_{\text{Ni}} = 0.56 \pm 0.05 M_\odot$, where the uncertainty of M_{Ni} also contains the estimated uncertainty of the distance modulus (~ 0.1 mag; see Section 3.2). Following Li et al. (2019), we find $\kappa = 0.19 \text{ cm}^2 \text{ g}^{-1}$, $M_{\text{ej}} = 0.99 M_\odot$, and $E_{\text{kin}} = 0.81$ for the mean opacity, ejecta mass, and kinetic energy, respectively. These values are within the range of typical SNe Ia as recently found by Scalzo et al. (2019) for a larger sample. From M_{ej} and E_{kin} , the average scaling velocity is $\sim 11,700 \text{ km s}^{-1}$, which agrees well with the observed Si II expansion velocity around maximum light ($\sim 11,200 \text{ km s}^{-1}$; see Section 4).

3.4. Early-Time Color Evolution

Following the discovery of SN 2017cfd shortly after explosion, KAIT was able to immediately obtain multiband data including B , V , C lear (similar to R), and I , thereby providing early-time colors.

Stritzinger et al. (2018a) found that there are two distinct populations of SNe Ia by examining the early-phase intrinsic $(B-V)_0$ color evolution of a dozen SNe Ia discovered very young. The “blue” group exhibits blue colors that evolve slowly, while the “red” group is characterized by red colors and evolves more rapidly, as shown

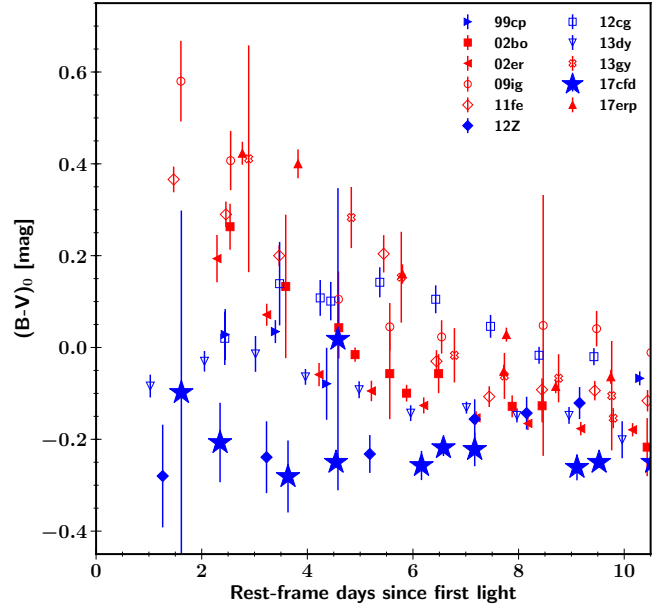


FIG. 5.— Similar to Figure 2 of Stritzinger et al. (2018a), showing the optical $(B-V)_0$ color evolution of SNe Ia discovered very young. Here we replot with a subset of the Stritzinger et al. (2018a) sample of those SN Ia that were discovered or observed by LOSS, including SN 2009ig, SN 2011fe, SN 2012cg, SN 2013dy, and SN 2013gy. We add six more from the LOSS sample (SN 1999cp, SN 2002bo, SN 2002er, SN 2012Z, SN 2017cfd, and SN 2017erp) and confirm that the two distinct early populations (“red” versus “blue”) presented by Stritzinger et al. (2018a) remain valid. SN 2017cfd belongs to the “blue” population.

in their Figure 2 (Stritzinger et al. 2018a).

In Figure 5, we replot their Figure 2 using a subset of the sample from Stritzinger et al. (2018a) of those SNe Ia that were discovered or observed by LOSS, including SN 2009ig, SN 2012cg, SN 2013dy, and SN 2013gy, as well as SN 2011fe (though not discovered by LOSS, KAIT/LOSS conducted follow-up observations at early times). Using the same criterion as Stritzinger et al. (2018a), namely to select SNe Ia that have early $(B-V)$ color data within three days of the FFLT, we add six additional LOSS SNe Ia that were not included in Stritzinger et al. (2018a) but have either old or new LOSS photometry published by Ganeshalingam et al. (2010) and Stahl et al. (2019a), including SN 1999cp, SN 2002bo, SN 2002er, SN 2012Z, SN 2017cfd, and SN 2017erp (though note that similar to SN 2011fe, the two objects SN 2002bo and SN 2017erp were not discovered by LOSS, but KAIT/LOSS had early-time follow-up observations). The parameters of these six new SNe Ia are given in Table 3.

TABLE 3
EARLY COLOR EVOLUTION PARAMETERS FOR SIX SNE Ia

SN(data ref.)	Host	Redshift	$E(B - V)_{\text{MW}}$	$E(B - V)_{\text{host}}$	t_{first} (JD or MJD)	Type	Color
1999cp(1)	NGC 5468	0.0103	0.025	0.022 ²	2451346.3 ²	normal	blue
2002bo(1,3)	NGC 3190	0.0053	0.027	0.430 ³	2452340.9 ²	normal	red
2002er(1)	UGC 10743	0.0090	0.142	0.218 ⁴	2452508.4 ²	normal	red
2012Z(5)	NGC 1309	0.0071	0.035	0.070 ⁶	55953.9 ⁷	Iax	blue
2017cfd(8)	IC 0511	0.01209	0.020	0.230 ⁸	57826.6 ⁸	normal	blue
2017erp(5)	NGC 5861	0.00674	0.095	0.150 ⁹	57916.5 ⁷	normal	red

(1) Ganeshalingam et al. (2010), (2) Zheng et al. (2017b), (3) Benetti et al. (2004), (4) Pignata et al. (2004), (5) Stahl et al. (2019a), (6) Stritzinger et al. (2015), (7) This work, using the method given by Zheng et al. (2017b), (8) This paper, (9) Brown et al. (2019). Reddening values are given in mag.

We then plot SN 2017cfd over this subset sample with a total of 11 SNe Ia observed by LOSS, as shown in Figure 5; open symbols represent the SNe from Stritzinger et al. (2018a), while filled symbols are the six new SNe, and SN 2017cfd is indicated with a filled star. Note that there is one data point for SN 2017cfd around 4.6 days that deviates from the evolution trend, caused by the bad quality of images on that night, but the measurement is largely consistent within the error bar. As one can see, with six more SNe added to the sample, we confirm that the two distinct early-time populations remain valid. SN 1999cp, SN 2012Z, and SN 2017cfd belong to the "blue" group, whose $(B - V)_0$ color evolves slowly at early times, similar to the other SNe Ia in the "blue" group. On the other hand, SN 2002bo, SN 2002er, and SN 2017erp are consistent with the "red" group. It is also interesting to note that the newly added SN 2012Z is the only SN Iax in both our new sample and the sample from Stritzinger et al. (2018a), and it is consistent with the "blue" group.

Stritzinger et al. (2018a) discussed various processes that may be contributing to the early-phase emission and the distinct grouping; these include interaction with a nondegenerate companion, the presence of high-velocity ^{56}Ni , interaction with circumstellar material, and opacity differences in the outer layers of the ejecta. They conclude that each explanation has its own defects (see also Jiang et al. 2018), thus requiring further theoretical modeling as well as gathering a larger sample of events. The LOSS discovery of SN 2017cfd is the latest event that can be added to this sample (LOSS discovered or observed about half of this ~ 20 SN Ia sample with early-time color data), and it would be interesting to see if this dichotomy persists with more data obtained in the future.

3.5. Progenitor Constraints

The very early-time observations constrain the emission from the ejecta, which can be used to limit the radius of the progenitor star, or the companion star if the ejecta collide with with a companion star (e.g., Kasen 2010). Such work has been applied to several SNe Ia, including SN 2011fe (Nugent et al. 2011; Bloom et al. 2012), SN 2012cg (Silverman et al. 2012b), SN 2013dy (Zheng et al. 2013), SN 2013gy (Holmbo et al. 2019), SN 2014J (Goobar et al. 2014), iPTF14atg (Cao et al. 2015), SN 2015F (Im et al. 2015), SN 2017cbv (Hosseinzadeh et al. 2017), SN 2018oh (Li et al. 2019), and SN 2019ein (Kawabata et al. 2019); these studies all ruled out a giant companion.

For SN 2017cfd, the earliest B -band observation of ~ 18.54 mag (corrected for extinction) at 1.6 d limits any emission from this process to be $\nu L_\nu \lesssim 8.7 \times 10^{40} \text{ erg s}^{-1}$ at optical wavelengths. Comparing these parameters with those of SN 2011fe (see Fig. 4 of Nugent et al. 2011) and scaling the analysis to match SN 2017cfd, we obtain an upper limit for the companion star radius to be $R_0 \lesssim 2.5 R_\odot$. This is not as stringent a constraint as that provided by the study of SN 2011fe, which has $R_0 \lesssim 0.1 R_\odot$, but our result for SN 2017cfd is consistent with those of other SN Ia studies that rule out a red-giant companion.

4. OPTICAL SPECTRA ANALYSIS

We obtained a total of 12 optical spectra of SN 2017cfd ranging from 3.5 d to 80 d after the FFLT. The first spectrum was taken 13.2 d before B maximum brightness. Figure 6 shows the full spectral sequence of SN 2017cfd.

We use the SuperNova Identification code (SNID; Blondin & Tonry 2007) to spectroscopically classify SN 2017cfd. For nearly all of the spectra, we find that SN 2017cfd is very similar to many normal SNe Ia. Thus, we conclude that SN 2017cfd is a spectroscopically normal SN Ia, consistent with the photometric analysis given in Section 3.

We examine the Na I D absorption feature, which is often converted into reddening (but with large scatter) through an empirical relationship (Poznanski et al. 2011; Stritzinger et al. 2018b). In several of our spectra with good signal-to-noise ratio, we clearly detect the blended Na I D at the redshifted wavelength of SN 2017cfd, but not at the rest-frame wavelength. From these spectra, we measure an averaged EW of Na I D to be $\text{EW} = 1.72 \pm 0.18 \text{ \AA}$ from the host galaxy. Using the best-fit relation from Stritzinger et al. (2018b), $A_V = (0.78 \pm 0.15) \times \text{EW}(\text{Na I D})$, we estimate a host-galaxy extinction of $A_V = 1.34 \pm 0.40$ mag, which corresponds to $E(B - V) = 0.45 \pm 0.13$ mag assuming $R_V = 3.1$. The foreground Milky Way extinction, on the other hand, is very small according to Schlafly & Finkbeiner (2011), only $E(B - V) = 0.02$ mag, consistent with the nondetection of Na I D in our spectra. However, since the Na I D EW method has large scatter, and the SN would appear to be too luminous if we adopt $A_V = 1.34$ mag estimated from the Na I D EW method, we instead adopt the extinction estimated from MLCS2k2 fitting with $A_V = 0.39 \pm 0.03$ mag and $R_V = 1.7$ as discussed in Section 3.2. Nevertheless, the Na I D EW method serves as independent evidence showing that SN 2017cfd suffers a certain amount of host-

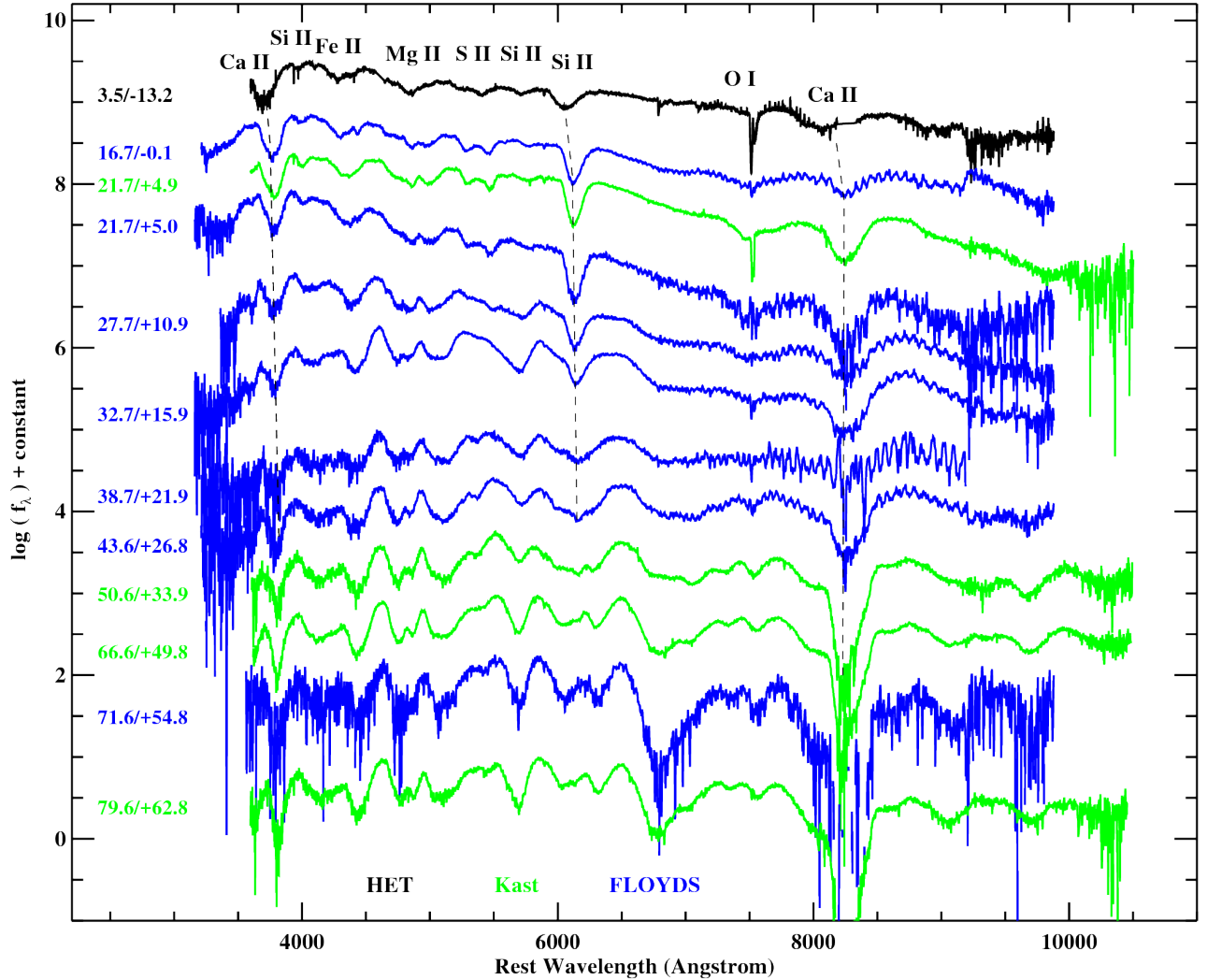


FIG. 6.— Spectral sequence of SN 2017cfd. Each spectrum is labeled with its age relative to both the FFLT and to B -band maximum light. Some major spectral features are labeled at the top. Spectra taken by different instruments are shown in different colors. In the first and third spectra from the top, telluric absorption is visible near 7600 Å (and a little near 6860 Å in the first spectrum). Dashed lines are meant to help guide the eye when examining absorption features.

galaxy extinction.

The spectra of SN 2017cfd exhibit absorption features from ions typically seen in SNe Ia including Ca II, Si II, Fe II, Mg II, S II, and O I. We do not find a clear C II feature, which is seen in over one-fourth of all SNe Ia (e.g., Parrent et al. 2011; Thomas et al. 2011; Folatelli et al. 2012; Silverman & Filippenko 2012), in the earliest spectrum of SN 2017cfd at phase -13.2 d. Although there appears to be a suspicious dip at the red edge of Si II $\lambda 6355$ that might be caused by C II $\lambda 6580$, this feature is very weak, not as clear as those seen in a few other SN Ia early-time spectra such as SN 2013dy (Zheng et al. 2013) and SN 2017cbv (Hosseinizadeh et al. 2017). Strong absorption features of Si II, including Si II $\lambda 4000$, Si II $\lambda 5972$, and Si II $\lambda 6355$, are clearly seen in all spectra, though the Si II $\lambda 5972$ feature in SN 2017cfd is relatively weak.

We then measure the individual line velocities from the minimum of the absorption features (see Silverman et al. 2012c, for details) and show them in Figure 7. As

expected, the velocities of all lines decrease from early phases to relative constancy around peak brightness, as seen in almost all SNe Ia. Specifically, the velocity of the Si II $\lambda 6355$ line decreases from $\sim 14,500 \text{ km s}^{-1}$ at discovery to $\sim 11,200 \text{ km s}^{-1}$ around maximum light, and then continues to decrease thereafter. Si II $\lambda 6355$ also has the largest velocity among all three Si II lines ($\lambda 4000$, $\lambda 5792$, and $\lambda 6355$). But Ca II H&K tends to exhibit the highest velocity among all the features, higher even than the Ca II near-infrared triplet, consistent with most SNe Ia. The strong absorption of Si II $\lambda 6355$ is commonly used to estimate the photospheric velocity; $\sim 11,200 \text{ km s}^{-1}$ at peak brightness is very typical of normal SNe Ia (e.g., Wang et al. 2013; Stahl et al. 2019b, submitted.).

5. CONCLUSIONS

In this paper we have presented optical photometric and spectroscopic observations of SN 2017cfd, which was discovered very young, with the first detection merely 1.6 ± 0.7 d after the FFLT. We find that SN 2017cfd is a

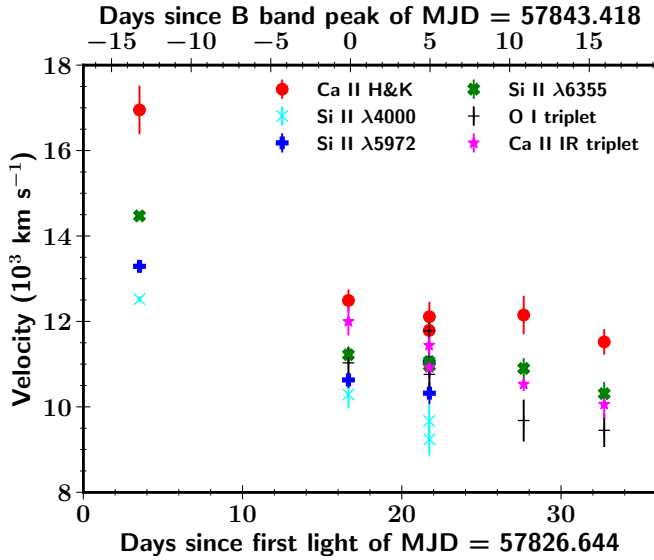


FIG. 7.— The expansion velocity evolution of different lines measured from the spectra of SN 2017cfd.

normal SN Ia in nearly every respect. (1) SN 2017cfd took ~ 16.8 d to reach B -band maximum, typical of SNe Ia. (2) There is a certain amount of host-galaxy extinction of SN 2017cfd based on the detection of Na I D lines from the host galaxy as well as the MLCS2k2 light-curve fitting method; however, considering that the Na I D EW method has large scatter, we adopt the extinction estimated from MLCS2k2 fitting with $A_V = 0.39 \pm 0.03$ mag and $R_V = 1.7$. After extinction correction, its maximum brightness has a normal luminosity, $B = -19.2 \pm 0.2$ mag. (3) An estimated $\Delta m_{15}(B)$ value of 1.16 mag along with spectral information supports its normal SN Ia classification. (4) SN 2017cfd has a Si II $\lambda 6355$ velocity of $\sim 11,200$ km s $^{-1}$ at peak brightness, also very typical of normal SNe Ia.

SN 2017cfd was detected very early. There are currently fewer than ~ 20 SNe Ia with color data in the first three days, and fewer than a dozen SNe Ia with color data in the first two days. Using the early-time photometry, we are able to constrain the companion star radius to be $\lesssim 2.5 R_\odot$, ruling out a red-giant companion associated with SN 2017cfd. We also find that the

intrinsic $(B - V)_0$ color evolution of SN 2017cfd at very early times belongs to the "blue" population, consistent with the dichotomy of the "red" and "blue" populations at early phases. Therefore, thanks to the early discovery and photometric follow-up, SN 2017cfd remains valuable at this stage for building up a bigger sample for studying SNe Ia at very early times. A significantly larger sample is being obtained with available new facilities (e.g., the Zwicky Transient Facility; ZTF), and with future new telescopes there will be many such discoveries (e.g., the Large Synoptic Survey Telescope).

During the final completion stages of this manuscript, Yao et al. (2019) released high-quality light curves of 127 SNe Ia discovered by ZTF in 2018, and a large fraction of their sample may have $(g - r)$ color data in the first three days. However, since their analysis use phase measurements relative to the g -band maximum instead of the FFLT, a direct comparison cannot be made with our analysis. A reanalysis to find the FFLT from the Yao et al. (2019) sample is required but is beyond the scope of this paper.

A.V.F.'s group at U.C. Berkeley is grateful for financial assistance from Gary & Cynthia Bengier, the Christopher R. Redlich Fund, the TABASGO Foundation, and the Miller Institute for Basic Research in Science (U.C. Berkeley). We thank the staffs of the various observatories at which data were obtained. This work makes use of observations from the LCO network. KAIT and its ongoing operation were made possible by donations from Sun Microsystems, Inc., the Hewlett-Packard Company, AutoScope Corporation, Lick Observatory, the NSF, the University of California, the Sylvia & Jim Katzman Foundation, and the TABASGO Foundation. Research at Lick Observatory is partially supported by a generous gift from Google. This work is part of the project "Transient Astrophysical Objects" GINOP 2.3.2-15-2016-00033 of the National Research, Development, and Innovation Office (NKFIH), Hungary, funded by the European Union.

REFERENCES

- Benetti, S., Meikle, P., Stehle, M., et al. 2004, MNRAS, 348, 261
 Blondin, S., & Tonry, J. L. 2007, ApJ, 666, 1024
 Bloom, J., Kasen, D., Shen, K., et al. 2012, ApJL, 744, L17
 Brown, T. M., Baliber, N., Bianco, F. B., et al. 2013, PASP, 125, 1031
 Brown, P. J., Hosseinzadeh, G., Jha, S. W., et al. 2019, ApJ, 877, 152
 Cao, Y., Kulkarni, S. R., Gal-Yam, A., et al. 2016, ApJ, 832, 86
 Cao, Y., Kulkarni, S. R., Howell, D. A., et al. 2015, Nature, 521, 328
 Chonis, T. S., Hill, G. J., Lee, H., et al. 2014, SPIE, 91470A, 1
 Chonis, T. S., Hill, G. J., Lee, H., et al. 2016, SPIE, 99084C, 1
 de Vaucouleurs, G., de Vaucouleurs, A., Corwin, H. G., Jr., Buta, R. J., Paturel, G., & Fouqué, P. 1991, RC3.9, "Third Reference Catalogue of Bright Galaxies," version 3.9 (New York: Springer)
 Falco, E. E., Kurtz, M. J., Geller, M. J., et al. 1999, PASP, 111, 438
 Filippenko, A. V. 1982, PASP, 94, 715
 Filippenko, A. V. 1997, ARA&A, 35, 309
 Filippenko, A. V. 2005, in 1604–2004, Supernovae as Cosmological Lighthouses, ed. M. Turatto, et al. (San Francisco: ASP), 87
 Filippenko, A. V., Li, W. D., Treffers, R. R., & Modjaz, M. 2001, in Small-Telescope Astronomy on Global Scales., ed. B. Paczyński, W. P. Chen, & C. Lemme (San Francisco: ASP), 121
 Foley, R. J., Scolnic, D., Rest, A., et al. 2018, MNRAS, 475, 193
 Ganeshalingam, M., Li, W., Filippenko, A. V., et al. 2010, ApJS, 190, 418
 Goobar, A., Johansson, J., Amanullah, R., et al. 2014, 784, L12
 Guevel, D., & Hosseinzadeh, G. 2017, dguevel/PyZOGY: Initial release (Version v0.0.1). Zenodo.
 Guy, J., Astier, P., Baumont, S., et al. 2007, A&A, 466, 11
 Hachisu, I., Kato, M., & Nomoto, K. 1996, ApJL, 470, L97
 Hicken, M., Wood-Vasey, W. M., Blondin, S., et al. 2009, ApJ, 700, 1097
 Hillebrandt, W., & Niemeyer, J. C. 2000, ARA&A, 38, 191
 Holmbo, S., Stritzinger, M. D., Shappee, B. J., et al. 2019, A&A, 627, A174
 Hosseinzadeh, G., Sand, D., Valenti, S., et al. 2017, 845, 11
 Hoyle, F., & Fowler, W. A. 1960, ApJ, 132, 565

- Iben, I., Jr., & Tutukov, A. V. 1984, *ApJS*, 54, 335
- Im, M., Choi, C., Yoon, S., et al. 2015, *ApJS*, 221, 22
- Jiang, J., Doi, M., Maeda, K., & Shigeyama, T., 2018, *ApJ*, 865, 149
- Jha, S., Maguire, K., & Sullivan, M. 2019, *Nature*, 3, 706
- Jha, S., Riess, A. G., & Kirshner, R. P. 2007, *ApJ*, 659, 122
- Kawabata, M., Maeda, K., Yamanaka, M., et al. 2019, *arXiv:1908.03001*
- Kasen, D. 2010, *ApJ*, 708, 1025
- Leaman, J., Li, W., Chornock, R., & Filippenko, A. V. 2011, *MNRAS*, 412, 1419
- Li, W., Filippenko, A. V., Chornock, R., & Jha, S. 2003, *PASP*, 115, 844
- Li, W., Wang, X., Vinko, J., et al. 2019, *ApJ*, 870, 12
- Maeda, K., Jiang, J., Shigeyama, T. & Doi, M. 2018, *ApJ*, 861, 78
- Magee, M. R., Sim, S. A., Kotak, R. & Kerzendorf, W. E. 2018, *A&A*, 614, A115
- Meng, X., Chen, X., & Han, Z., et al. 2009, *MNRAS*, 395, 2103
- Miller, J. S., & Stone, R. P. S. 1993, *Lick Obs. Tech. Rep.* 66 (Santa Cruz: Lick Obs.)
- Nugent, P. E., Sullivan, M., Cenko, S. B., et al. 2011, *Nature*, 480, 344
- Pakmor, R., Kromer, M., Taubenberger, S., Sim, S. A., Röpke, F. K., & Hillebrandt, W. 2012, *ApJL*, 747, L10
- Papadogiannakis, S., Goobar, A., Amanullah, R., et al. 2019, *MNRAS*, 483, 5045
- Perlmutter, S., Aldering, G., Goldhaber, G., et al. 1999, *ApJ*, 517, 565
- Phillips, M. M. 1993, *ApJ*, 413, L105
- Pignata, G., Patat, F., Benetti, S., et al. 2004, *MNRAS*, 355, 178
- Piro, A. L., & Nakar, E. 2013, *ApJ*, 769, 67
- Piro, A. L., & Nakar, E. 2014, *ApJ*, 784, 85
- Polin, A., Nugent, P. & Kasen, D. 2019, *ApJ*, 873, 84
- Poznanski, D., Ganeshalingam, M., Silverman, J. M., & Filippenko, A. V. 2011, *MNRAS*, 415, L81
- Rabinak, I., Livne, E., & Waxman, E. 2012, *ApJ*, 757
- Riess, A. G., Casertano, S., Yuan, W., et al. 2018, *ApJ*, 855, 136
- Riess, A. G., Casertano, S., Yuan, W., et al. 2019, *ApJ*, 876, 85
- Riess, A. G., Filippenko, A. V., Challis, P., et al. 1998, *AJ*, 116, 1009
- Röpke, F. K., Kromer, M., Seitenzahl, I. R., et al. 2012, *ApJL*, 750, L19
- Scalzo, R. A., Parent, E., Childress, M., et al. 2019, *MNRAS*, 483, 628
- Schlafly, E. F., & Finkbeiner, D. P. 2011, *ApJ*, 737, 103
- Shivvers, I., Filippenko, A. V., Silverman, J. M., et al. 2019, *MNRAS*, 482, 1545
- Silverman, J. M., Foley, R., Filippenko, A. V., et al. 2012a, *MNRAS*, 425, 1789
- Silverman, J. M., Ganeshalingam, M., Cenko, S. B., et al. 2012b, *ApJ*, 756, L7
- Silverman, J. M., Kong, J. J., & Filippenko, A. V. 2012c, *MNRAS*, 425, 1819
- Stahl, B. E., Zheng, W., de Jaeger, T., et al. 2019a, in press (*arXiv:1909.11140*)
- Stahl, B. E., Zheng, W., de Jaeger, T., et al. 2019b, submitted
- Stetson, P. B. 1987, *PASP*, 99, 191
- Stritzinger, M. D., Shappee, B., Piro, A., et al. 2018a, *ApJ*, 864, L35
- Stritzinger, M. D., Taddia, F., Burns, C. R., et al. 2018b, *A&A*, 609, 135
- Stritzinger, M. D., Valenti, S., Hoefflich, P., et al. 2015, *A&A*, 573, 2
- Tonry, J. L., Stubbs, C. W., Lykke, K. R., et al. 2012, *ApJ*, 750, 99
- Valenti, S., Howell, D. A., Stritzinger, M. D., et al. 2016, *MNRAS*, 459, 3939
- Wang, X., Wang, L., Filippenko, A. V., Zhang, T., & Zhao, X. 2013, *Science*, 340, 170
- Webbink, R. F. 1984, *ApJ*, 277, 355
- Yao, Y., Miller, A. A., Kulkarni, S. R., et al. 2019, *arXiv:1910.02967*
- Zackay, B., Ofek, E. O., & Gal-Yam, A. 2016, *ApJ*, 830, 27
- Zheng, W., & Filippenko, A. V. 2017, *ApJ*, 838, L4
- Zheng, W., Filippenko, A. V., Mauerhan, J., et al. 2017a, *ApJ*, 841, 64
- Zheng, W., Kelly, P., & Filippenko, A. V. 2017b, *ApJ*, 848, 66
- Zheng, W., Kelly, P., & Filippenko, A. V. 2018, *ApJ*, 858, 104
- Zheng, W., Shivvers, I., Filippenko, A. V., et al. 2014, *ApJ*, 783, L24
- Zheng, W., Silverman, J. M., Filippenko, A. V., et al. 2013, *ApJ*, 778, L15